Hindawi
Shock and Vibration
Volume 2020, Article ID 3824216, 20 pages
https://doi.org/10.1155/2020/3824216

Research Article

Identification of Sudden Stiffness Change in the Acceleration Response of a Nonlinear Hysteretic Structure

Sheng-Lan Ma,[1,2] **Shao-Fei Jiang**,[3] **Chen Wu**,[1] **and Si-Yao Wu**[3]

[1]*Fujian Provincial Key Laboratory of Advanced Technology and Informatization in Civil Engineering, Fuzhou 350108, China*
[2]*CSCEC Strait Construction and Development Co., Ltd., Fuzhou 350015, China*
[3]*College of Civil Engineering, Fuzhou University, Fuzhou 350108, China*

Correspondence should be addressed to Shao-Fei Jiang; cejsf@fzu.edu.cn

Received 30 May 2019; Revised 2 October 2019; Accepted 4 November 2019; Published 31 January 2020

Guest Editor: Franco Concli

The integration of discrete wavelet transform and independent component analysis (DWT-ICA) method can directly identify time-varying changes in linear structures. However, better metrics of structural seismic damage and future performance after an event are related to structural permanent and total plastic deformations. This study proposes a two-stage technique based on DWT-FastICA and improved multiparticle swarm coevolution optimization (IMPSCO) using a baseline nonlinear Bouc–Wen structural model to directly identify changes in stiffness caused by damage as well as plastic or permanent deflections. In the first stage, the measured structural dynamic responses are preprocessed firstly by DWT, and then the Fast ICA is used to extract the feature components that contain the damage information for the purpose of initially locating damage. In the second stage, the structural responses are divided at the identified damage instant into segments that are used to identify the time-varying physical parameters by using the IMPSCO, and the location and extent of damage can accordingly be identified accurately. The efficiency of the proposed method in identifying stiffness changes is assessed under different ground motions using a suite of two different ground acceleration records. Meanwhile, the effect of noise level and damage extent on the proposed method is also analyzed. The results show that in a realistic scenario with fixed filter tuning parameters, the proposed approach identifies stiffness changes within 1.25% of true stiffness within 8.96 s; therefore, it can work in real time. Parameters are identified within 14% of the actual as-modeled value using noisy simulation-derived structural responses. This indicates that, in accordance with different demands, the proposed method can not only locate and quantify damage within a short time with a high precision but also has excellent noise tolerance, robustness, and practicality.

1. Introduction

Civil engineering structures are subjected to continuous structural deterioration caused by aging, low-cycle fatigue loads from smaller earthquakes, and daily environmental loading. Therefore, the severity of deterioration needs to be monitored periodically in order to ensure structural integrity and safety [1]. If damage is detected in the early stage, maintenance works will be carried out timely with low cost. For this purpose, structural responses (e.g., accelerations) due to structural vibrations induced by external loading are on-time collected by structural health monitoring (SHM) systems; analyzing and processing collected structural response is a popular way to identify, locate, and quantify structural damage based on the principle that damage affects the mechanical properties of the structure (i.e., stiffness and damping), which will change structural dynamic properties (e.g., frequencies and model shapes) [2, 3].

A further approach to damage detection is the identification of an anomaly in the time history. A number of researchers have been able to locate an anomaly in the processed signal that is related to damage by using signal processing techniques [4], which often combine frequencies and time domains (such as wavelet analysis [5], empirical mode decomposition, and blind source separation). These approaches mainly aim to detect the anomaly in online or real-time structural health monitoring. For example, Yang and Nagarajaiah [6] proposed a unsupervised blind source

separation technique, which combined wavelet transform and independent component analysis (ICA), for the sake of detecting damage instant for linear structure. In addition, Jiang et al. [7] employed wavelet transform combined with data fusion to identify structural damage anomaly in time domain for linear structures. Generally, the majority of proposed damage instant detection methods are used to identify linear structures. Unfortunately, when structures are subjected to earthquake excitation, nonlinearity widely exists in these damaged structures [8]. For instance, when damage occurs in reinforced concrete structures, cracks opening and closing under dynamic excitation are typical nonlinear process which leads to the hysteretic performance of the structures [9].

After completing the structural response novelty detection in time history due to sudden stiffness change, it is necessary to use an accurate and fast approach to identify the degree of the stiffness changed and the parameters in nonlinear hysteretic system for urgent postevent response and decision making. Therein, the particle swarm optimization (PSO) algorithm, due to its excellent characteristics of simple principle and fast convergence, is widely applied in system identification [10], damage detection [11, 12], and sensor optimization placement [13] in linear structure, as well as in parameters identification [14] in nonlinear hysteretic structure. The principle of optimization-based identification consists in minimizing the difference between experimentally and numerically obtained structural dynamic properties. However, the standard PSO algorithm may get trapped in the local optimum and might not converge to the global optimum. In order to improve the performance of standard PSO algorithm, some investigation was made by combining PSO algorithm with other algorithm and modifying the inertia weights. By introducing some mechanism into standard PSO algorithm, Charalampakis and Dimou [15] presented two variants of PSO algorithm to identify the Bouc–Wen hysteretic system. Furthermore, Zhang and Xia [16] developed an improved PSO algorithm by defining a fitness function to identify parameters of nonlinear dynamic hysteretic models. Overall, the fitness functions for parameters identification based on PSO algorithm mainly utilized modal information. However, due to the significant computational complexity and longer runtime, the applications of aforementioned methods for real-time or time varying damage detection are limited.

Due to the fact that few methods can not only detect structural response novelty but also identify structural damage severity in nonlinear structures, this paper focuses on developing an approach that will capture a nonlinear behavior in time domain to detect structural response novelty firstly and then utilize an optimization algorithm, with fitness function in time domain, to identify structural parameters and structural stiffness in less time. The first question that arises is how to characterize a nonlinear response as mentioned above. This has been addressed in a wide range of mechanical and civil engineering applications via signal processing methods like Hilbert–Huang transform-based [1, 17], Wavelet transform-based [7], neural network-based [18, 19], and independent component analysis-based methods [20]. Yang and Nagarajaiah [6] combined wavelet transform with independent component analysis (ICA) to detect linear structural instant, which had excellent robustness. As the extension of Reference [6], this paper firstly utilized the integration of discrete wavelet transform and independent component analysis (DWT-ICA) to detect nonlinear structural response novelty. The second question that arises is how to quickly and accurately identify nonlinear structural stiffness and finally to achieve the aim of detecting sudden stiffness change. Just as the aforementioned study and the authors' previous study [21], an improved multiparticle swarm coevolution optimization algorithm (IMPSCO) with time-domain fitness function is applied to detect nonlinear structural damage by the first time. All in all, this paper presents a two-stage technique based on DWT-FastICA and the improved multiparticle swarm coevolution optimization (IMPSCO) using a baseline nonlinear Bouc–Wen structural model to directly identify sudden stiffness changes in the acceleration response.

The organization of the paper is as follows. Section 2 reviews the basic theory of the Bouc–Wen model. Section 3 numerically and experimentally demonstrates the feasibility of IMPSCO algorithm to identify time-varying nonlinear structural parameters. Section 4 depicts the damage detection strategy based on DWT-FastICA and IMPSCO algorithm. Numerical simulations of two-DOF nonlinear hysteretic system are carried out in Section 5, and Section 6 gives the concluding remarks finally.

2. Bouc–Wen Model: Model Formulation and Parameter Constraints

Structural dynamic behavior must generally be taken into account in the design of mechanical systems to insure their performance and reliability [22]. In structural systems, hysteresis appears as a natural mechanism in the materials used and produces restoring forces that dissipate energy. Hysteresis, as used here, refers to the memory nature of inelastic structural behaviors where the restoring force depends not only on the instantaneous deformations but also on the history of the deformations. The detailed analytical modeling of this behavior results in very complicated nonlinear models that are not suitable for sudden stiffness change. One of the most common semiphysical models proposed is the first-order nonlinear differential equation known as the Bouc–Wen model. More specifically, a nonlinear frame structure with passive MR dampers under seismic base motion, as shown in Figure 1, can be modeled as follows [23]:

$$\mathbf{M}\ddot{X}(t) + \mathbf{C}\dot{X}(t) + \mathbf{R}(\mathbf{X}, \mathbf{Z}, t) = -\mathbf{F}(t), \tag{1}$$

where $\mathbf{M}$ and $\mathbf{C}$ are the mass and damping matrices of the system, respectively; $\mathbf{X}$, $\dot{X}$, and $\ddot{X}$ are displacement, velocity, and acceleration matrix of the base-isolation system, respectively; $\mathbf{F}$ is the external force; and $\mathbf{R}$ is the vector of restoring force governed by the following first-order differential equation from the so-called classical Bouc–Wen model:

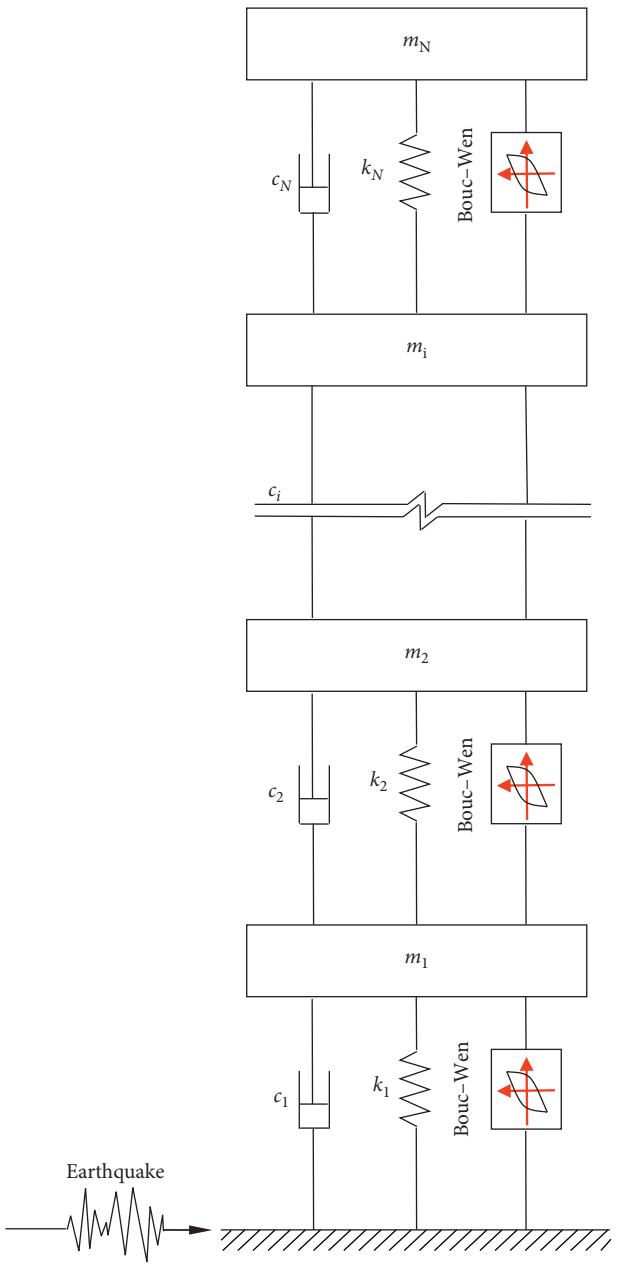

FIGURE 1: Model of a base-isolation system with passive MR dampers.

$$\mathbf{R}(\mathbf{X}, \mathbf{Z}, t) = \left[R_1 - R_2, R_2 - R_3, \cdots, R_{N-1} - R_N\right]^{\mathrm{T}}, \tag{2}$$

in which

$$\begin{aligned} \mathrm{R}_i &= \alpha_i k_i X_i(t) + (1-\alpha_i) k_i Y_i Z_i(t), \\ \dot{Z}_i(t) &= \frac{1}{Y_i}\left\{A_i \dot{X}_i(t) - \left(\beta_i \left|\dot{X}_i(t)\right| Z_i(t) \left|Z_i(t)\right|^{n_i-1} \right.\right. \\ &\quad \left.\left. + \gamma_i \dot{X}_i(t) \left|Z_i(t)\right|^{n_i}\right)\right\}, \\ A_i &> 0,\ \beta_i > 0,\ -\beta_i < \gamma_i < \beta_i,\ n_i \geq 1, \end{aligned} \tag{3}$$

where k is the stiffness of the system; A, β, γ, and n are stiffness, loop fatness, loop pinching, and abruptness parameters in the classical Bouc–Wen model, respectively; α is the bilinear factor, defined as the ratio of the post- to preyield stiffness of the system; Y is the yield displacement of the system; $Z(t)$ is the dimensionless Bouc–Wen hysteresis component; the subscript i represents the i-th story; and N is the total number of stories.

It is noted that n is the power factor which determines the sharpness of the curve from elastic to plastic force-deflection behavior of the system.

In this paper, we assume structural state vector $\mathbf{S}$ as follows:

$$\mathbf{S} = \left[\mathbf{X},\ \ddot{X},\ \mathbf{Z}\right]. \tag{4}$$

Therefore, equation (1) can be transformed as a first-order ordinary differential equation as follows:

$$\dot{\mathbf{S}} = \left[\dot{\mathbf{X}},\ \ddot{X},\ \dot{\mathbf{Z}}\right] = f(\mathbf{S}). \tag{5}$$

Therein,

$$\ddot{X} = M^{-1}\left[\mathbf{F}(t) - \mathbf{C}\dot{X}(t) - \mathbf{R}(\mathbf{X}, \mathbf{Z}, t)\right]. \tag{6}$$

As a result, if we initialized structural state vector, equation (6) can be solved by the fourth-order Runge–Kutta method [24] to calculate structural dynamic responses.

3. Feasibility of IMPSCO Algorithm Applied in Identification of Nonlinear Structural Parameters

In order to identify time-varying nonlinear structural parameters, the improved multiparticle swarm coevolution optimization (IMPSCO) algorithm is applied, which is further used to locate and quantify structural damage as well as identify the parameters in the Bouc–Wen model.

3.1. Theory of the IMPSCO Algorithm. For basic multiparticle swarm coevolution optimization algorithm (MPSCO) [25], multiple subpopulations are divided into two layers. All particles from the upper layer follow the optimum of the entire population so as to obtain a faster convergence speed, while all particles from the lower layer follow the optimum of the subpopulation to ensure the population diversity. Although the performance of basic MPSCO is better than standard PSO in some respects, the subpopulations in the lower layer still perform the process of standard PSO, which makes particle falling into the local optimum possible. To solve this problem, we proposed the IMPSCO algorithm, and the details can be seen in Reference [21], and it was applied to locate and quantify damage in a linear structure. Figure 2 shows the flowchart of the IMPSCO algorithm.

Wherein, the key point in IMPSCO is worst particle replacement. More specially, when the particle is recorded as the worst for the predetermined times I_{w}, replace it with local center of gravity G_g:

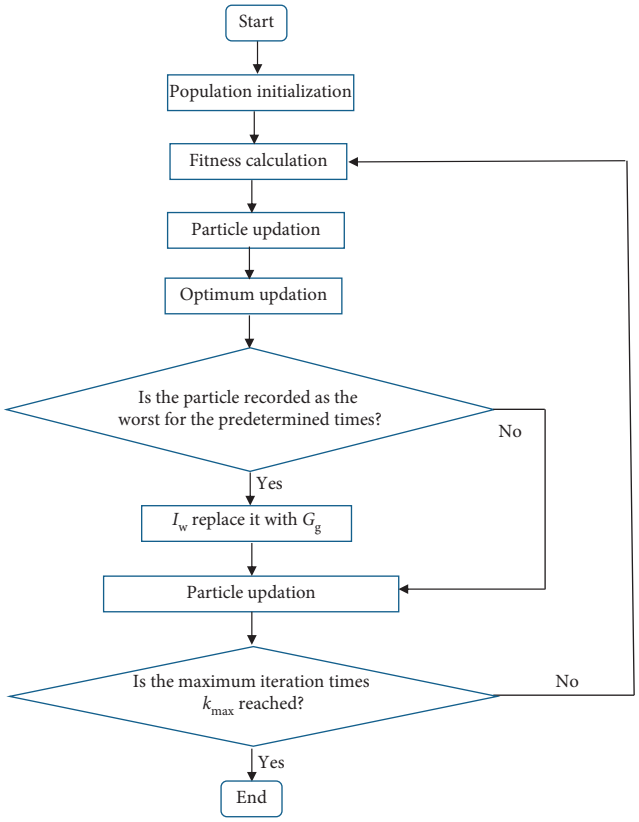

Figure 2: The flowchart of the IMPSCO algorithm.

$$G_g = \frac{\sum_{i=1}^{s} z_i}{s}, \tag{7}$$

where s and z_i represent the number of the selected excellent particles and their position, respectively.

The most important task for optimization is to determine the fitness function in the IMPSCO. A useful fitness function not only has high accuracy but also needs less runtime, which are the main evaluation indices of the optimization algorithm for detecting sudden structural stiffness change. In addition, some parameters in the nonlinear hysteretic model may have little effects on the shape of the hysteretic curve. Therefore, we utilized the difference between the calculated and testing accelerations as the fitness function value, which contains lots of structural sensitive information. However, it is difficult to calculate the minimum. We employed the reciprocal of the mean square error (MSE) between the reproduced acceleration responses $\ddot{X}(t \mid p)$ and the reference measured acceleration responses $\ddot{X}(t)$ and replaced the mean square error (MSE) between them as the fitness function. When cast in discrete form, it can be expressed as

$$\max f(\theta) = \frac{1}{\sum_{i=1}^{N}\sum_{k_l=1}^{L}\left(\ddot{X}_i\left(t_{k_l}\right) - \ddot{X}_i\left(t_{k_l} \mid p\right)\right)^2}, \tag{8}$$

where $\boldsymbol{\theta}$ is the structural parameters vector to be optimized; N is the total number of measuring points; and L is the length of time history.

3.2. Feasibility: Numerical Simulation

3.2.1. Model Description. To evaluate the performance of IMPSCO algorithm applied to identification of nonlinear hysteretic base-isolation systems, a realistic base-isolated system is created as shown in Figure 3 [26]. The numerical model can be simplified as a two degree-of-freedom (DOF) structure. Its basic definition includes the following: mass of each floor: $m_1 = m_2 = 1\,\text{kg}$; initial stiffness of each floor: $k_1 = k_2 = 102.64\,\text{N/m}$; damping coefficients of each floor: $\zeta_1 = \zeta_2 = 2\%$; parameters in the classical Bouc–Wen model: $A = 1; \beta = 0.5; \gamma = 0.5; n = 2; \alpha = 0.1$; the yield displacement of the system: $Y = 0.045\,\text{m}$; and the basic period of structure: $T = 1\,\text{s}$.

Meanwhile, according to the sensitivity analysis of the parameters in the classical Bouc–Wen model listed in Reference [26], we assumed that some parameters with low sensitivity are constants in some cases in order to reduce the identified parameters in IMPSCO and simply the identification process. In summary, this study considered four cases with different parameters known. In addition, the search range of each parameter ($\boldsymbol{\theta}$) is within the interval of [0.5**b**, 2**b**], where **b** is the theoretical value of the corresponding parameter ($\boldsymbol{\theta}$).

In this study, the structure was subjected to El-Centro earthquake wave, Kobe earthquake wave, and Northridge earthquake wave, respectively, at the base, as shown in Figure 3. In order to reduce the particle dimension of IMPSCO, four cases were simulated to observe the feasibility of IMPSCO algorithm, as shown in Table 1. Therefore, by setting the sampling frequency of 50 Hz and the loading time $t = 30\,\text{s}$, the structural acceleration responses were calculated by using the classical fourth-order Runge–Kutta algorithm [24].

To consider the operating environment, Gaussian white noise with different levels was added to all structural responses and the earthquake motion. The structural responses were then represented as

$$y_i = y_i^a \times (1 + \varepsilon R), \tag{9}$$

where y_i and y_i^a represent the contaminated and theoretical signals, respectively; R is a normally distributed random variable with zero mean and a derivation of 1; and ε is an index representing the noise level.

Therefore, the signal-to-noise ratio (SNR) is defined as

$$\text{SNR} = 20\log_{10}\left(\frac{1}{\varepsilon}\right) = 20\log_{10}\left(\frac{A_{\text{signal}}}{A_{\text{noise}}}\right), \tag{10}$$

where A_{signal} and A_{noise} are the amplitudes of the signal and noise, respectively.

In this paper, the SNR was 30 dB.

3.2.2. Identification Process. In order to identify parameters of 2-DOF structure, two issues need to be ensured for the IMPSCO algorithm: encoding parameters and initial setting parameters. The details can be seen as follows.

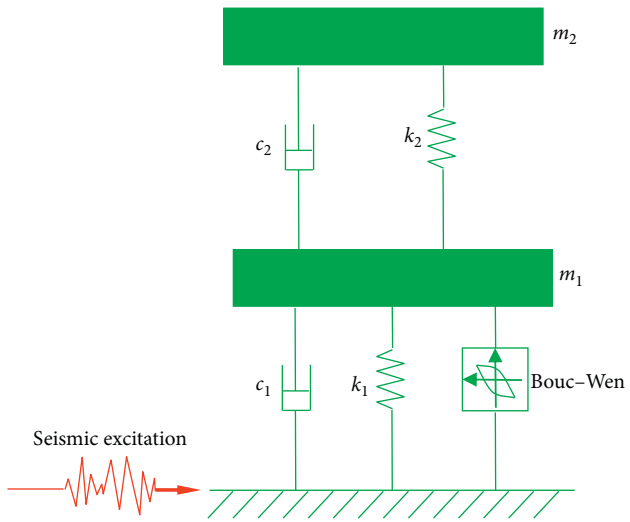

Figure 3: 2-DOF structure with Bouc–Wen model subjected to seismic excitation.

Table 1: Different cases for simulation.

Cases	Unknown parameters	Known parameters
S1	$k_1, k_2, \zeta_1, \zeta_2, Y, \alpha, \beta, \gamma, n$	—
S2	$k_1, k_2, \zeta_1, \zeta_2, Y, \alpha, \beta, n$	$\gamma = 0.5$
S3	$k_1, k_2, \zeta_1, \zeta_2, Y, \beta, n$	$\alpha = 0.1; \gamma = 0.5$
S4	$k_1, k_2, \zeta_1, \zeta_2, Y, \alpha, \beta, \gamma$	$n = 2$

(1) Parameter Encoding Involved in the IMPSCO. This study assumed that the mass of each floor was known. Therefore, the parameters encoded in the IMPSCO were initial stiffness (k_1, k_2) and damping coefficients (ζ_1, ζ_2), yield displacement (Y) of the first floor, bilinear factor (α), loop fatness (β), loop pinching (γ), and abruptness parameters (n) in the classical Bouc–Wen model system, and the details could be seen in Figure 4. Consequently, the number of subpopulations m was 9.

(2) Parameters in IMPSCO. To maximize the fitness function using IMPSCO presented in Section 3.1, some parameters should be set and initialized in advance for IMPSCO. Generally, 3~5 subpopulations with 30 to 100 particles in total were sufficient. The inertia weight w was set linearly varying from 0.9 to 0.4 and learning factors c_1 and c_2 were set to 2 simultaneously. In addition, the limited times for the worst record I_w and the number of the selected excellent particles s were both empirically set to 5~10, respectively. Finally, the parameters of IMPSCO in this study were initialized as shown in Table 2.

3.2.3. Identification Results and Discussion. According to the process described in Section 3.1, the responses shown in Figure 5 were employed to identify the parameters in the nonlinear structure and in Bouc–Wen model system. The results are listed in Table 3, and relative errors between identified results and theoretical values are shown in Table 4.

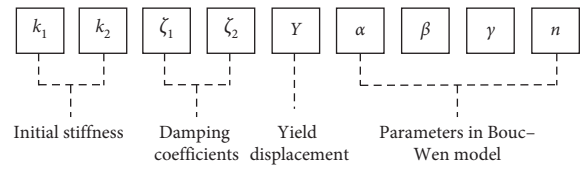

Figure 4: The parameters encoded in the IMPSCO.

Table 2: Specifications of IMPSCO algorithm.

Parameter	Description	Value
mm	The total number of subpopulations	3
nn	The size of a subpopulation	10
c_1	Cognitive parameter	2
c_2	Social parameter	2
$\rho^{\min}$	Minimum of inertia weight	0.4
$\rho^{\max}$	Maximum of inertia weight	0.9
I_w	Limited times for worst record	5
S	The number of the selected excellent particles	6
$I_{\max}$	The maximum iteration times	200

The following conclusions and remarks can be made from the two tables:

(1) The relative errors of initial stiffness of system (k) and the abruptness parameter (n) in the classical Bouc–Wen model are less than 3.5%, and the rest of identified parameters have lower computational accuracy. More specifically, the maximum relative errors for stiffness (α), loop fatness (β), and loop pinching (γ) are 10.00% (S1, S2, S4), 22.00% (S1), and 22.00% (S1, S4), respectively; the corresponding values are 10.22% (S1), 1.93% (S2), 1.36% (S3), and 6.18% (S4) for the yield displacement (Y); in addition, the maximum relative errors for damping coefficients (ζ_1 and ζ_2) are 8.50% (S1), 19.00% (S2), 14.00% (S3), and 8.50% (S4), respectively.

There are two reasons for this phenomenon. The first one is that when we used the error between reproduced and measured acceleration responses as the fitness function, the stiffness of the system mainly influences the reproduced accelerations. By contrast, the damping coefficients have little effect on the reproduced accelerations. As a result, it is difficult to accurately identify the damping coefficients. The second reason is that, as presented in Reference [27], the abruptness parameter in the classical Bouc–Wen model (n) is a power factor, which changes the smoothness of transition from elastic region to plastic region in the hysteretic versus actual displacement curves, with little change in the acceleration response. Correspondingly, the remaining three parameters in the classical Bouc–Wen model are not sensitive to accelerations.

(2) It is accurate to identify stiffness of the system (k_1, k_2) and the abruptness parameter (n) in the classical Bouc–Wen model by using IMPSCO with

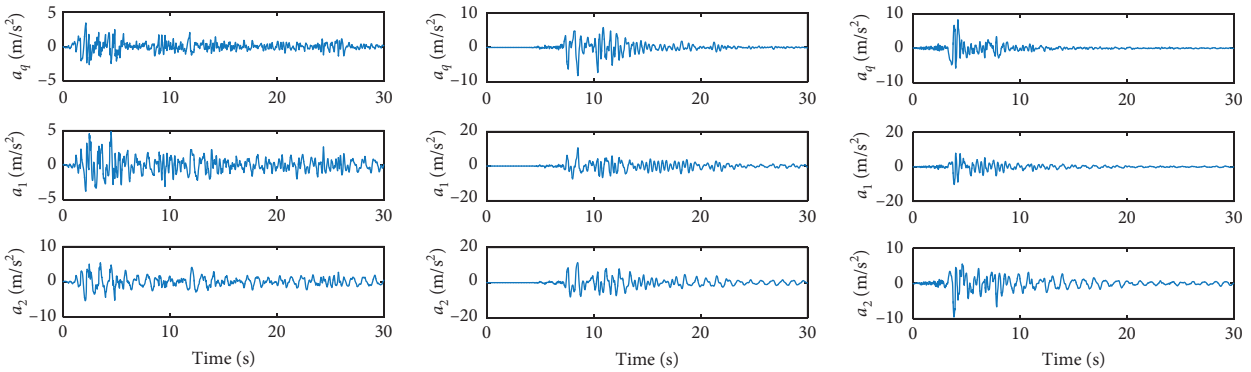

Figure 5: Acceleration responses of the simulated structure under different earthquake waves, $^*a_1$ is the acceleration responses of the first floor; a_2 is the acceleration responses of the second floor; a_q is corresponding earthquake excitation. (a) El-Centro earthquake waves. (b) Kobe earthquake waves. (c) Northridge earthquake waves.

Table 3: Identification results of the simulated structure subjected to the different earthquake excitation in different cases.

Case	Seismic excitation	k_1 (N/m)	k_2 (N/m)	ζ_1 (%)	ζ_2 (%)	Y (mm)	α	β	γ	n
S1	(a) El-Centro earthquake	102.45	102.73	1.86	2.06	46.46	0.09	0.55	0.52	2.06
	(b) Kobe earthquake	102.79	102.73	2.12	1.83	47.38	0.10	0.56	0.57	1.95
	(c) Northridge earthquake	103.01	102.58	1.96	1.98	49.60	0.10	0.61	0.61	1.97
S2	(a) El-Centro earthquake	103.15	102.46	2.09	2.16	44.13	0.11	0.47	—	2.01
	(b) Kobe earthquake	102.65	102.74	2.12	1.82	44.65	0.10	0.49	—	1.96
	(c) Northridge earthquake	101.46	103.09	2.38	2.09	45.19	0.10	0.46	—	2.07
S3	(a) El-Centro earthquake	102.86	102.70	2.03	2.24	44.70	—	0.48	—	2.01
	(b) Kobe earthquake	103.13	102.71	2.15	1.84	44.39	—	0.48	—	1.93
	(c) Northridge earthquake	102.72	103.01	2.28	2.05	44.71	—	0.46	—	1.97
S4	(a) El-Centro earthquake	103.06	102.55	2.08	2.17	47.78	0.11	0.55	0.61	—
	(b) Kobe earthquake	102.54	102.73	2.16	1.84	47.62	0.10	0.56	0.58	—
	(c) Northridge earthquake	102.94	102.65	2.16	2.01	46.23	0.10	0.52	0.56	—

Table 4: The relative errors between identified parameters and actual model parameters.

Case	Seismic excitation	Relative error (%)								
		k_1	k_2	ζ_1	ζ_2	Y	α	β	γ	n
S1	(a) El-Centro earthquake	0.19	0.09	7.00	3.00	3.24	10.00	10.00	4.00	3.00
	(b) Kobe earthquake	0.15	0.09	6.00	8.50	5.29	0.00	12.00	14.00	2.50
	(c) Northridge earthquake	0.36	0.06	2.00	1.00	10.22	0.00	22.00	22.00	1.50
	Average values	0.23	0.08	5.00	4.17	6.25	3.33	14.67	13.33	2.33
S2	(a) El-Centro earthquake	0.50	0.18	4.50	8.00	1.93	10.00	6.00	—	0.50
	(b) Kobe earthquake	0.01	0.10	6.00	9.00	0.78	0.00	2.00	—	2.00
	(c) Northridge earthquake	1.15	0.44	19.00	4.50	0.42	0.00	8.00	—	3.50
	Average values	0.55	0.24	**9.83**	7.17	1.04	3.33	5.33	—	2.00
S3	(a) El-Centro earthquake	0.21	0.06	1.50	12.00	0.67	—	4.00	—	0.50
	(b) Kobe earthquake	0.48	0.07	7.50	8.00	1.36	—	4.00	—	3.50
	(c) Northridge earthquake	0.08	0.36	14.00	2.50	0.64	—	8.00	—	1.50
	Average values	0.26	0.16	**7.67**	7.50	0.89	—	5.33	—	1.83
S4	(a) El-Centro earthquake	0.41	0.09	4.00	8.50	6.18	10.00	10.00	22.00	—
	(b) Kobe earthquake	0.10	0.09	8.00	8.00	5.82	0.00	12.00	16.00	—
	(c) Northridge earthquake	0.29	0.01	8.00	0.50	2.73	0.00	4.00	12.00	—
	Average values	0.27	0.06	6.67	5.67	4.91	3.33	8.67	16.67	—

the parameter listed in Table 2. Furthermore, for four cases (with different parameters to be identified and different particle dimension of IMPSCO), all the parameters of the nonlinear structure can be basically identified by IMPSCO. Although the identified results for the parameters in the classical Bouc–Wen model have lower accuracy than that of stiffness, the IMPSCO algorithm is suitable for identification of sudden stiffness change in actual structure. Just as shown in Table 4, the overall ranking for stiffness (k_1, k_2) and damping coefficients (ζ_1, ζ_2) is S1 > S4 > S3 > S2, and the overall ranking for remaining parameters is S3 > S2 > S4 > S1. This indicates that for all the parameters unknown case (S1), the identified results for the stiffness and damping have excellent accuracy. By contrast, the identified results for the parameters in the Bouc–Wen model have lower accuracy than other cases. However, the maximum error in the identification process is less than 16.7%. These error values are well within construction errors. It also demonstrates that the IMPSCO algorithm is applicable for detecting structural damage induced by stiffness change in structures.

3.3. Feasibility: Experiment

3.3.1. Test Setup. A MR damper test [27] was presented to further validate the proposed IMPSCO algorithm. The test's configuration schematic and the photograph of the testing system are shown in Figure 6.

It is noted that the modified Bouc–Wen model is superior in describing the force-displacement relationship of MR damper. Its expression is as follows:

$$\begin{aligned} F &= c\dot{x} + kx + \alpha z + f_0, \\ \dot{z} &= A\dot{x} - \left(\beta|\dot{x}|z|z|^{n-1} + \gamma\dot{x}|z|^n\right), \end{aligned} \tag{11}$$

where F and f_0 are the damping force and initial damping force; c and k are damping and the stiffness of the system, respectively; α is the bilinear factor, defined as the ratio of the post- to preyield stiffness of the system; and z is the dimensionless Bouc–Wen hysteresis component.

In testing processes, the actuator of the loading device was controlled by displacement input with a sinusoidal waveform as follows:

$$u = A_p \sin(2\pi ft), \tag{12}$$

where A_p is the displacement amplitude; f is the excitation frequency; and t is the loading time.

The main parameters of the MR damper are listed in Table 5.

In order to verify the effectiveness of the IMPSCO algorithm, four cases were simulated and discussed here. The details can be seen in Table 6. Herein, the electricity value was set as1.2 A and the excitation frequency was 0.1 Hz.

3.3.2. Identification Process. As described in Section 3.1, the parameters to be identified should be encoded first. It is noted that the stiffness in the modified Bouc–Wen model (A) was redundant, demonstrated by Worden and Becker [28] using principled Bayesian approach, and thus A was set to 1. The search range of other corresponding parameters are listed in Table 7.

Due to the fact that there was no acceleration record during the experiment, the error between measured displacement and produced displacement was set as the fitness function (equation (13)) and the parameters of IMPSCO in this study were the same as those in Section 3.2.2.

$$\max f(\theta) = \frac{1}{\sum_{i=1}^{N}\sum_{k_l=1}^{L}\left(X_i\left(t_{k_l}\right) - X_i\left(t_{k_l} \mid p\right)\right)^2}, \tag{13}$$

where $X(t)$ and $X(t \mid p)$ are the reference measured displacement and the reproduced displacement, respectively.

3.3.3. Identification Results and Discussion. According to the process described in Section 3.2.2, we utilized the experimental displacement as described in Figure 7 to identify the parameters in the modified Bouc–Wen model. The identification results are presented in Table 8.

Due to the fact that it is difficult to measure the values of the parameters in the modified Bouc–Wen model matched with the MR damper, the identification results listed in Table 8 were used to reconstruct the curve of displacements and damping forces so as to evaluate the efficiency of the proposed IMPSCO algorithm. The results are also shown in Figure 8. Herein, the identified values are also plotted in the same figure to compare with the measured ones.

It can be seen from Figures 7 and 8 that (1) the errors between identified values and measured ones for case 1 are much larger than those for cases 2, 3 and 4; (2) the identified values agree well with experimental values when the amplitude is larger than 5 mm, namely, cases 2, 3 and 4; and (3) the identified displacements coincide better with the measured values. The reason for the former is that when the amplitude of the MR damper is 5 mm, the damper just enter into the nonlinear phase. This implies that the modified Bouc–Wen model is not very suitable for simulating the MR damper in this early stage. By contrast, when the amplitude of the MR damper is larger than 5 mm and the MR damper comes into nonlinear phase, the identified results match well with experimental results. It is concluded that when the MR damper comes into the nonlinear phase, the modified Bouc–Wen model as described in equation (11) is perfect in depicting the force-displacement hysteretic relationship of the MR damper. In addition, the proposed IMPSCO algorithm is applicable to identifying parameters in the modified Bouc–Wen model.

4. Two-Stage Identification Strategy for Sudden Stiffness Change in Nonlinear Hysteretic Structures

The improved MPSCO algorithm is able to identify structural stiffness, but it cannot detect when the structure

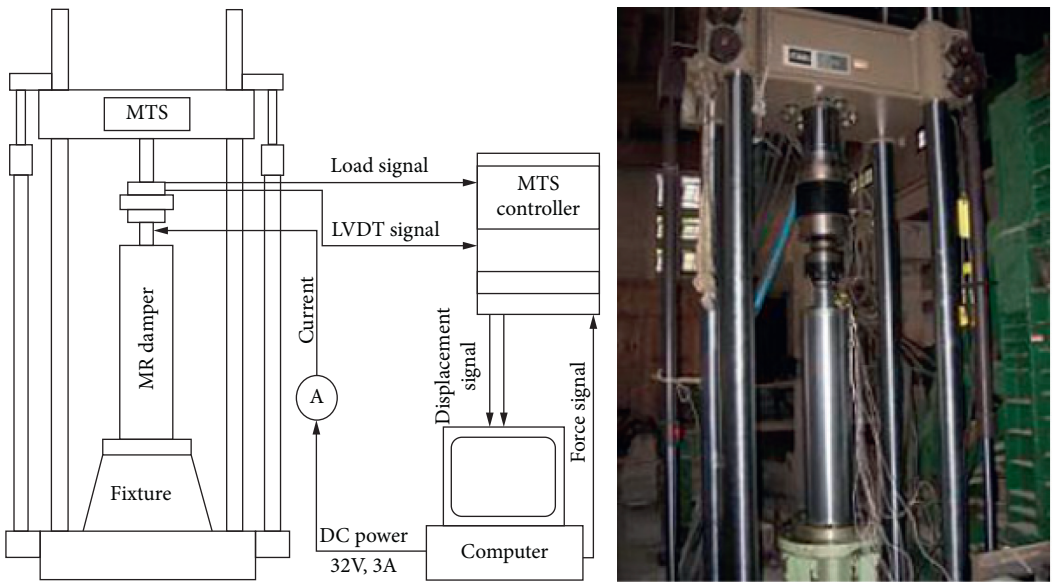

Figure 6: MR damper performance test setup [27].

Table 5: The main parameters of the MR damper.

Parameters	Values
Stroke (mm)	±50
External diameter of cylinder (mm)	194
Internal diameter of cylinder (mm)	160
Diameter of the piston rod (mm)	80
Effective length of the piston (mm)	250
Coil ($n \times$ turns)	5×840
Height of the annular flow path (mm)	2
Trench diameter of coil (mm)	110
Coil resistance (Ω)	5×8.1

Table 6: Different cases for the MR damper experiment.

Case	Amplitude (mm) (A_p)
Case 1	5
Case 2	10
Case 3	20
Case 4	30

Table 7: The parameters encoded in the IMPSCO for the MR damper experiment.

Parameters	Description	Initial range of parameters
f_0	Initial damping force	$[0, 30000]$
c	Damping of MR damper	$[0, 1.5 \times 10^8]$
k	Stiffness of MR damper	$[0, 3 \times 10^8]$
α	Bilinear factor defined as the post- to preyield stiffness ratio of the system	$[0, 3 \times 10^8]$
β	The loop fatness of the system	$[0, 30]$
γ	The loop pinching of the system	$[0, 30]$
n	The abruptness parameter of the system	$[0, 30]$

stiffness changed. As a result, a new two-stage damage detection strategy by integrating DWT-FastICA and the IMPSCO algorithm is proposed to identify the sudden stiffness change of the acceleration response in a nonlinear hysteric structure. The schematic diagram of the damage detection strategy is depicted in Figure 9. In the first stage, the measured structural dynamic responses are preprocessed firstly by discrete wavelet transform (DWT), and then the fast independent component analysis (Fast ICA) is employed to detect the structural response abnormality and initially locate damage location. In the second stage, the structural responses are divided into segments which are used to identify the time-varying nonlinear structural parameters by the IMPSCO algorithm, whereby the damage location and extent can be identified accurately.

4.1. The First Stage: Primary Damage Assessment. Two essential tasks in the first stage are detecting damage novelty and initially locating damage.

4.1.1. Separation of Wavelet Detailed Components. To complete the damage novelty detection, the time-series dynamic responses is preprocessed by DWT in order to separate the wavelet detailed components. DWT [29] is a useful tool for time-frequency analysis, which achieves multiresolution analysis of a signal by decomposing it into high-frequency (detail) and low-frequency (approximation) components at each level. If a signal is decomposed into LL levels, it can be reconstructed by

$$\ddot{X}(t) = \sum_{\mathrm{ll}=1}^{\mathrm{LL}} \ddot{X}_d^{\mathrm{ll}}(t) + \ddot{X}_a^{\mathrm{LL}}(t) = \sum_{\mathrm{ll}=1}^{\mathrm{LL}} \sum_{kk=-\infty}^{\infty} d_{\mathrm{kk,ll}} \psi_{\mathrm{kk,ll}}(t) + \sum_{\mathrm{kk}=-\infty}^{\infty} c_{\mathrm{kk,LL}} \phi_{\mathrm{kk,LL}}(t), \tag{14}$$

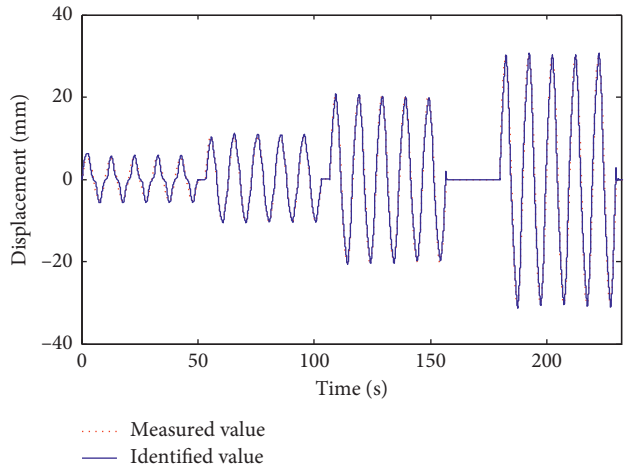

Figure 7: Comparison between identified displacements and measured ones.

Table 8: Identification results for the MR damper experiment.

Case	c (N·s/m)	k (N/m)	α	β	γ	N	f_0 (N)
Case 1	1.22×10^7	1.76×10^7	6.76×10^5	16.51	16.39	15.70	3286.92
Case 2	1.38×10^7	8.02×10^6	2.42×10^6	18.12	12.81	23.96	3668.17
Case 3	9.95×10^6	3.60×10^6	4.80×10^5	4.53	6.33	28.94	3000.00
Case 4	7.31×10^6	1.90×10^6	4.73×10^5	5.65	8.55	29.53	3000.00

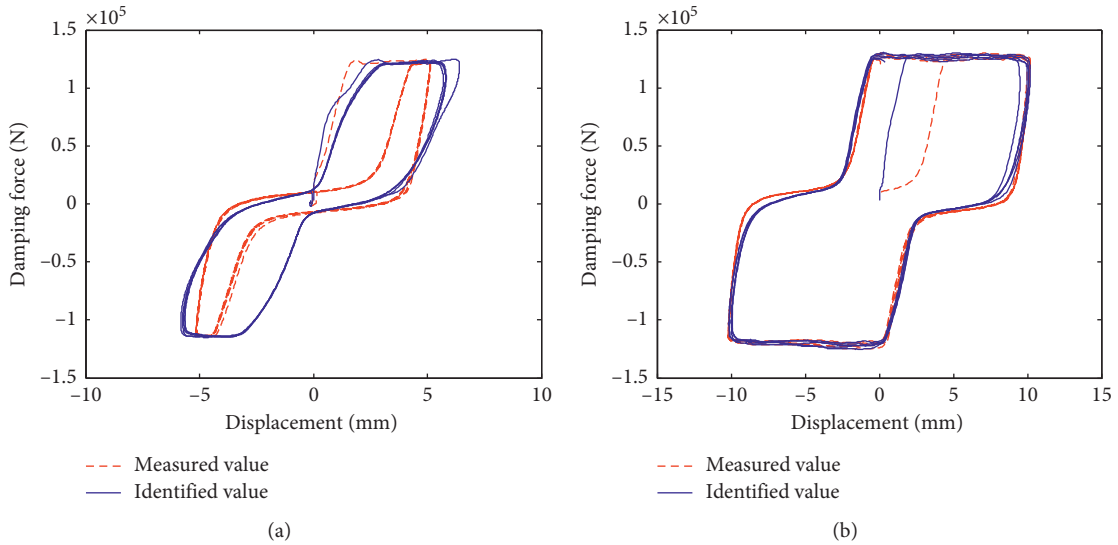

Figure 8: Continued.

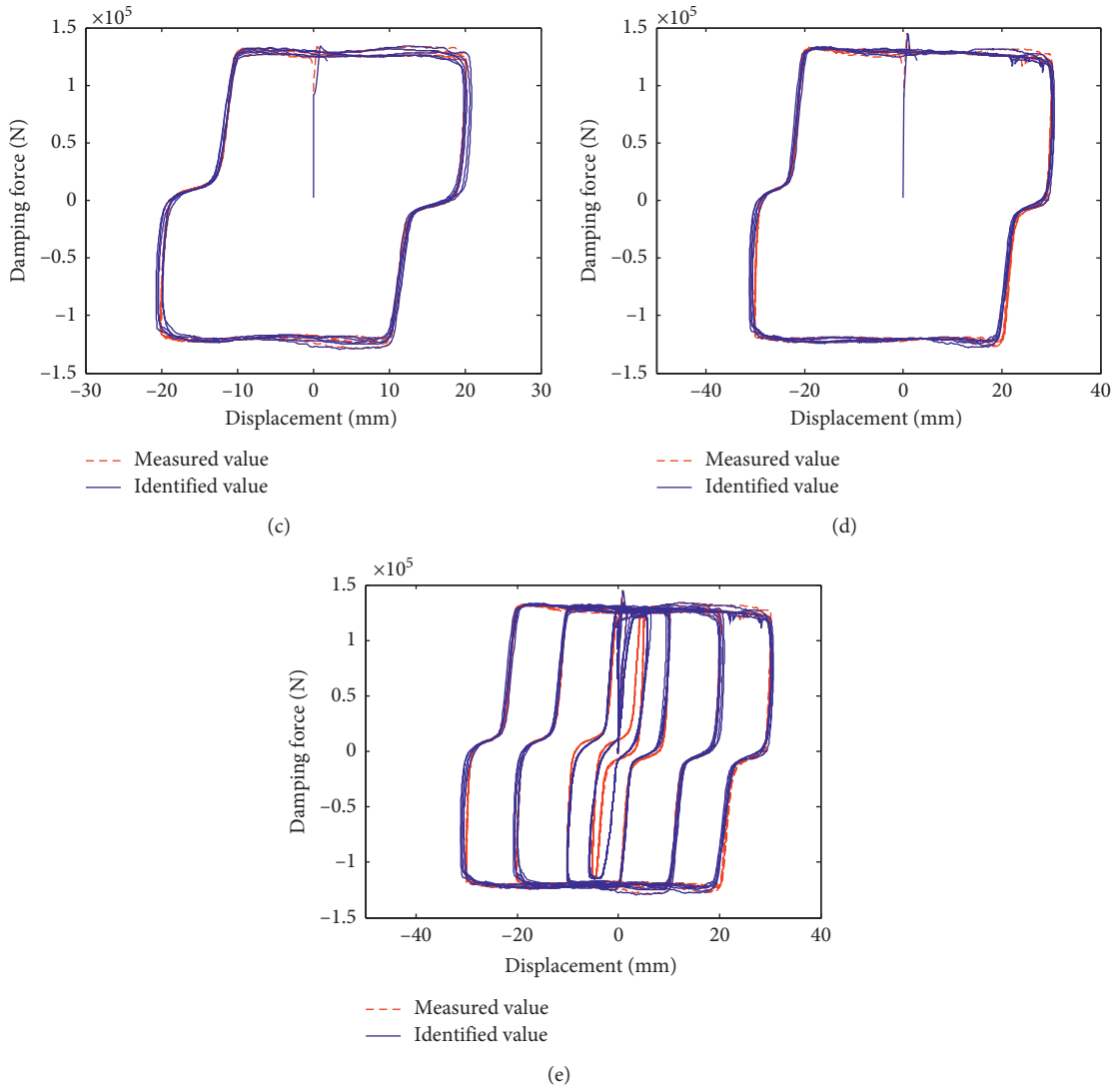

FIGURE 8: Comparison between identified values and measured values. (a)A_p = 5 mm. (b)A_p = 10 mm. (c)A_p = 20 mm. (d)A_p = 30 mm. (e) General damping force vs displacement curve.

where $\ddot{X}_d^{\mathrm{ll}}(t)$ is the detailed component at the *ll*-th scale level; $\ddot{X}_a^{\mathrm{LL}}(t)$ is the approximated component at the LL-th scale level; kk and ll are the translation and scale parameters, respectively; $d_{\mathrm{kk,ll}}$ and $\psi_{\mathrm{kk,ll}}(t)$ are the detail coefficient and wavelet function at the ll-th scale level, respectively; and $c_{\mathrm{kl,LL}}$ and $\phi_{\mathrm{kk,LL}}(t)$ are the approximation coefficient and scaling function at the LL-th scale level, respectively.

Two parameters should be predetermined using DWT to detect the singularity (or discontinuity points) of a signal. The first one is selecting the proper wavelet basis and the other one is the decomposition level involving in DWT. After determining the parameters, DWT is, respectively, performed in the structural dynamic responses X_i ($i = 1, 2, \ldots, m$; m is the total number of sensors) measured from each sensor location. Consequently, the wavelet detailed components wX_i on a certain scale which contain the most damage information can be separated, respectively. So, the wavelet detailed signal matrix can be built as $\mathbf{wX} = [wX_1, wX_2, \ldots, wX_m]^{\mathrm{T}}$.

4.1.2. Extraction of Feature Independent Component. A new singularity analysis method called DWT-ICA by integrating DWT with independent component analysis (ICA) was recently proposed and applied to structural damage detection. This method shows excellent performance in identifying sudden stiffness change for linear structures [6]. Independent component analysis (ICA) [30] is a computational technique for feature extraction in signal processing, which can separate a multivariate observed signal to statistically independent sources. It can be specially described as

$$\mathbf{wX}(t) = \mathbf{AwS}(t), \tag{15}$$

where $\mathbf{wS}(t) = [wS_1(t), \ldots, wS_m(t)]$ represents an n-dimensional independent source matrix and $\mathbf{A}$ represents an $m \times n$ $(m \geq n)$ mixing matrix.

The principle of ICA can be summarized as an optimization process to search for proper estimation of the

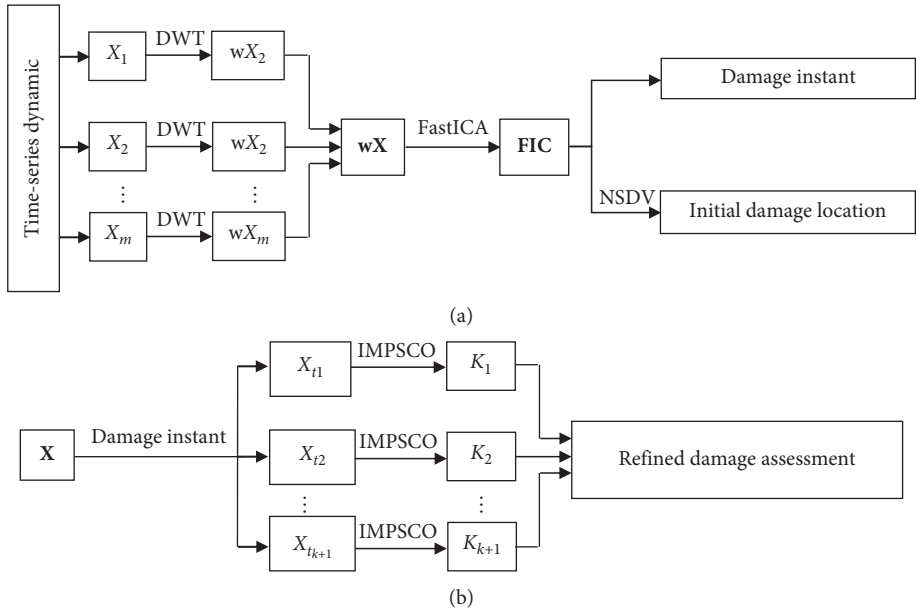

Figure 9: Two-stage sudden stiffness change of nonlinear structure detection strategy. (a) The first stage: primary damage assessment. (b) The second stage: refined damage assessment.

inverse of **A** (i.e., demixing matrix **W**) such that the source signal matrix **wS** can be recovered by

$$\mathbf{wS}(t) = \mathbf{WwX}(t). \tag{16}$$

Therefore, there are two key issues in the ICA: (1) the proper objective function in order to decide whether the obtained source signals are statistically independent; (2) the effective algorithm to implement the optimization of the objective function.

The Fast ICA proposed by Hyvärinen and Oja [31] is one of the most efficient and popular algorithms in revised ICA. It is based on a fixed-point iteration scheme maximizing non-Gaussianity as the objective function.

To extract the damage information hidden in the noisy wavelet-domain signals, the detailed signal matrix **wX** is processed by using the Fast ICA, thereby n_{IC} independent components IC_j ($j = 1, 2, \ldots, n_{\mathrm{IC}}$) can be obtained. Subsequently, the feature independent component (FIC) which contains the spike property can be extracted, and the position of the spike in the time history indicates the damage occurrence instant.

4.1.3. Initial Localization of Damage. After conducting the Fast ICA, the wavelet detailed signal matrix **wX** can be reconstructed by

$$\mathbf{wX} = \mathbf{A} \times \mathbf{IC} = \sum_{i=1}^{n} \mathbf{a_j} \cdot \mathrm{IC}_j, \tag{17}$$

where $a_j = [a_{1j}, \ldots, a_{ij}, \ldots, a_{mj}]^{\mathrm{T}}$ is the mixing vector which is called as the source distribution vector (SDV). Herein, the element a_{ij} that is defined as the source distribution factor (SDF) represents the proportion of IC_j distributed in wX_i; IC_j is the j-th independent component extracted by the Fast ICA.

When IC_j contained structural singularity information, it is called the feature independent component (FIC_k $k = 1, 2, \ldots, h$). If a_{ij} is the largest among its SDV, it indicates its corresponding location, where the response measured in the i-th sensor location Xi contains the most FIC, is the possibly damaged location.

The SDV can be normalized further by equation (18). Thus, the structural damage can be initially localized by the maximum among the NSDV of the FIC.

$$\begin{aligned} \mathbf{NS\,DF} &= \left[\mathrm{NSDF}_1, \mathrm{NSDF}_2, \cdots, \mathrm{NSDF}_i, \mathrm{NSDF}_m\right]^T, \\ \mathrm{NSDF}_i &= \frac{\left|a_{ij}\right|}{\sum_{i=1}^{m}\left|a_{ij}\right|}, \quad (i = 1, 2, \ldots, m). \end{aligned} \tag{18}$$

4.2. Refined Damage Assessment. First, the original time-series responses are divided into $k_s + 1$ segments as $\ddot{X}_{t_1}, \ddot{X}_{t_2}, \ldots, \ddot{X}_{t_{k_s+1}}$ according to the damage instant identified through FIC_{ks}, $k_s = 1, 2, \ldots, h$.

Second, IMPSCO is performed on the $k_s + 1$ segment $\ddot{X}_{t_1}, \ddot{X}_{t_2}, \ldots, \ddot{X}_{t_{k_s+1}}$, respectively; thus, the damage location and extent can be identified precisely according to the stiffness variation at each time period.

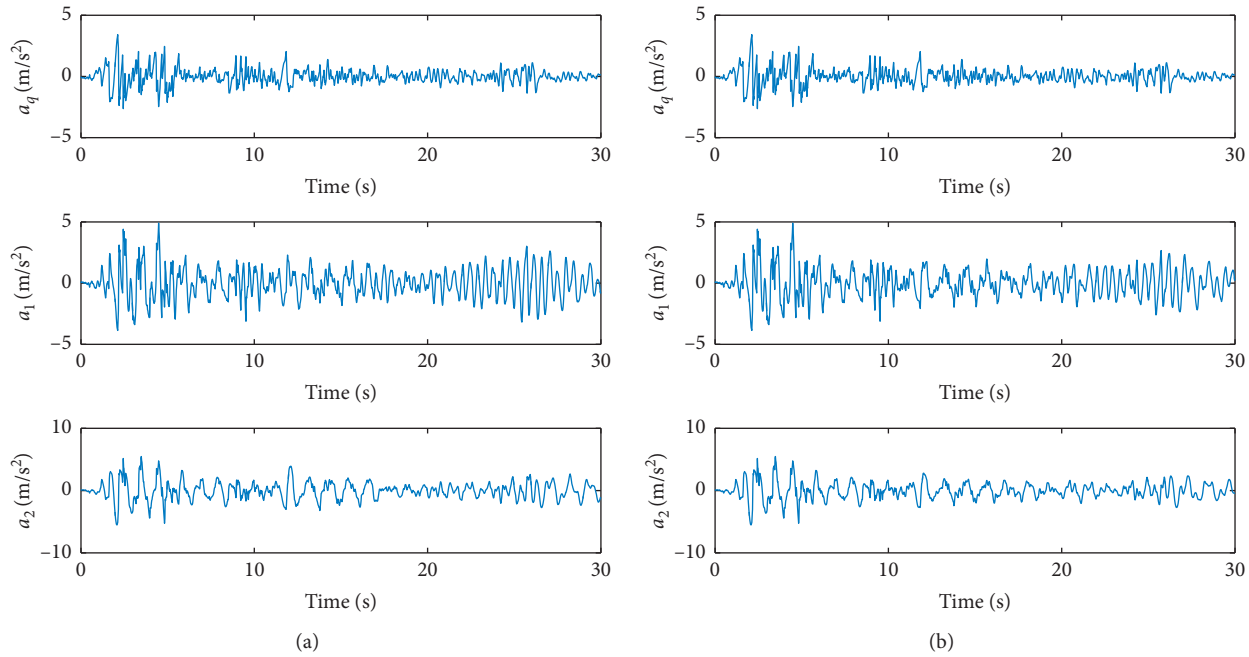

Figure 10: Original acceleration responses of the simulated structure under El-Centro earthquake wave. (a) Case 1. (b) Case 2.

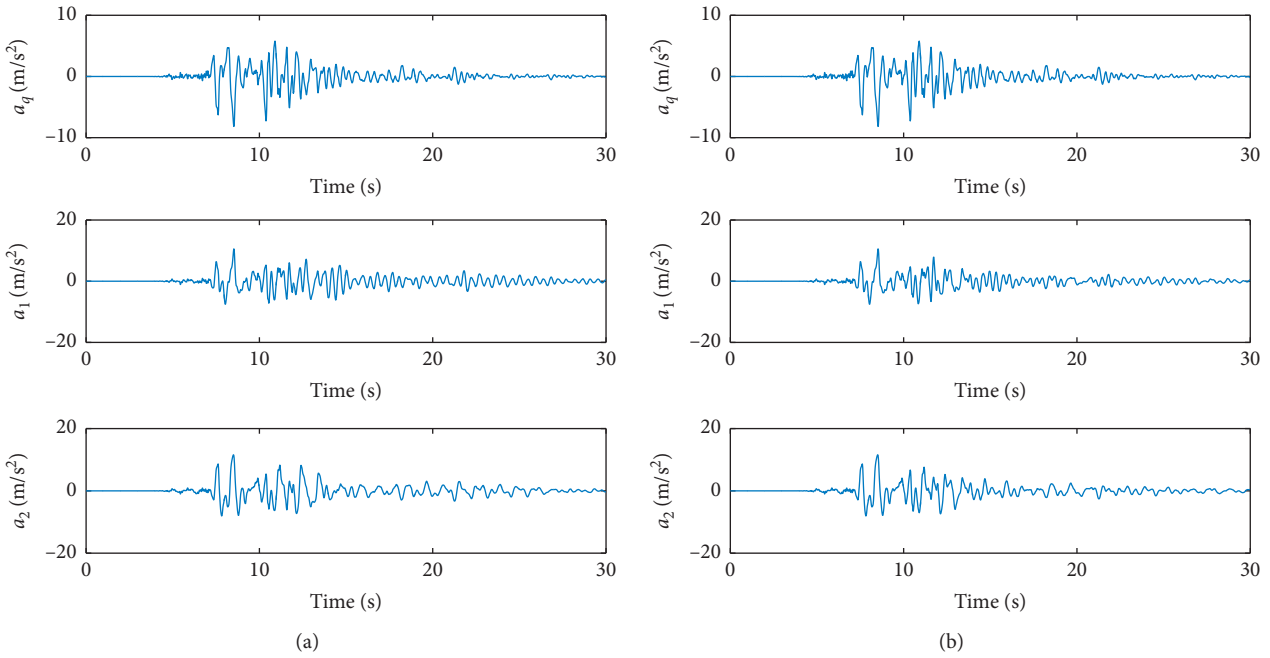

Figure 11: Original acceleration responses of the simulated structure under Kobe earthquake wave. (a) Case 1. (b) Case 2.

Table 9: Damage scenarios.

Damage scenario	Damage novelty, location, and extent
Case 1	$t = 10$ s, $k_2 = 102.64$ kN/m $\longrightarrow$ 61.58 kN/m
Case 2	$t = 10$ s, $k_1 = 102.64$ kN/m $\longrightarrow$ 71.85 kN/m $t = 20$ s, $k_2 = 102.64$ kN/m $\longrightarrow$ 71.85 kN/m

5. Numerical Study

5.1. Model Description. In order to validate the applicability and effectiveness of the proposed two-stage damage detection strategy for nonlinear structure, the nonlinear model presented in Section 2 was subjected to El-Centro earthquake excitation and Kobe earthquake excitation, respectively, at the base, as shown in Figure 3. The original acceleration responses are presented in Figures 10 and 11. As shown in Table 9, two damage cases with different damage novelty, location, and extent were simulated and discussed here. To approach the operating environment, Gaussian white noise with SNR = 30 dB is added to all the responses and the earthquake excitations as equation (10).

5.2. Damage Detection Model

5.2.1. The First Stage: Detect Structural Response Abnormality and Initially Locate Damage Location. Just as Section 4.1, the measured acceleration responses A_i ($i = 1, 2, 3$) were decomposed in single level by wavelet basis function db4, respectively. The corresponding detailed components $\mathrm{w}X_i$ ($i = 1, 2$) were then selected and built as the wavelet detailed signal matrix $\mathbf{wX} = [\mathrm{w}X_1, \mathrm{w}X_2]^T$. The Fast ICA is performed on $\mathbf{wX}$ to obtain the two independent components (IC_j ($j = 1, 2$)) and FICs. According to the position of spike in the FIC, the structural response novelty was identified, and the corresponding NSDV of the FIC was calculated via equation (18), and thus the damage location was initially estimated.

5.2.2. The Second Stage: Time-Varying Parameter Identification. The original acceleration responses A_i ($i = 1, 2$) were divided into several segments according to the obtained FICs, and then IMPSCO was employed to identify the structural parameters in each segment, respectively. In this example, the structural mass was assumed as known in advance; thus, the parameter vector to be optimized was $\theta = [k_1, k_2, c_1, c_2, n, \gamma, \alpha, \beta, Y]$. The search range of $\boldsymbol{\theta}$ was within the interval of $[0.5\mathbf{b}, 2\mathbf{b}]$, and $\mathbf{b}$ is the theoretical value of $\boldsymbol{\theta}$. Additionally, the IMPSCO parameters were set as listed in Table 2. Meanwhile, because the IMPSCO algorithm is a probabilistic optimization algorithm, the identification process was performed for ten times and the average values were regarded as final results to eliminate the influence of randomness. Finally, the structural damages were localized and quantified accurately depending on the stiffness variation in each time period.

5.3. Results and Discussion

5.3.1. Primary Damage Assessment. The results of wavelet detailed component separation are shown in Figures 12 and 13, and the feature independent components (FICs) extracted are shown in Figures 14 and 15, respectively.

It is seen that significant damage information can hardly be directly identified from the wavelet detailed components when the structure is subjected to the earthquake excitation. After the Fast ICA processing as shown in Figures 14 and 15, the FIC containing the spike is extracted obviously. More specifically, IC_2 is the FIC in case 1, and it indicates that the structure is probably damaged at $t = 10$ s because the spike occurs at $t = 10$ s under both earthquake motions. Similarly, in case 2, IC_2 can be used to estimate the occurring time of damage. It is found from Figure 15, as a consequence, that the structure is probably damaged at $t = 10$ s and $t = 20$ s, respectively.

After detecting structural response novelty, the damage can then be initially localized by the NSDV. For single-damage pattern, case 1, we utilized NSDV to initially locate structural damage in case 1 under both earthquake excitations. The results are shown in Figure 16. It can be seen that the maximum of NSDF corresponding to IC_2 occurs at the second story when the structure was subject to El-Centro and Kobe earthquake excitation, respectively. It indicates that the second story is probably damaged location when $t = 10$ s. It can be seen from Figure 15 (b) that for muti-damage pattern, Case 2, damage abnormal information contained in IC2. Therefore, it is difficult to locate structural damage. All in all, structural response novelty can be identified correctly, and for single damage pattern, damage can be located initially.

5.3.2. Refined Damage Assessment. When the primary damage assessment was completed, the IMPSCO was then used to implement segmentation parameters optimization and refined damage assessment. For case 1, the identification process was divided into two segments, namely, 0~10 s and 10~30 s; correspondingly, for case 2, the identification process is divided into three segments, namely, 0~10 s, 10~20 s, and 20~30 s. Furthermore, the IMPSCP is used to identify the structural stiffnesses and coefficients as well as the parameters in the Bouc–Wen model, such as stiffness (A), loop fatness (β), loop pinching (γ), and abruptness parameters (n), and the results are shown in Figures 17 and 18. Tables 10 and 11 list the errors between identification results and theoretical values under different earthquake waves. It is found that the identification accuracy is very high for structural stiffnesses. More specifically, the maximum errors for the structural stiffness are 0.93% and 1.08% under EI-Centro earthquake wave, respectively. By contrast, the maximum errors are 0.51% and 1.25% under Kobe earthquake wave, respectively. On the contrary, except story stiffness, the rest of identified parameters have lower accuracy, but the maximum errors are no more than 12% and 14%, under two different earthquake waves. These error values basically met the requirements of engineering needs. In addition, difference in the maximum error values under the different ground motions used is due to differences in the structural responses induced by different earthquake damage.

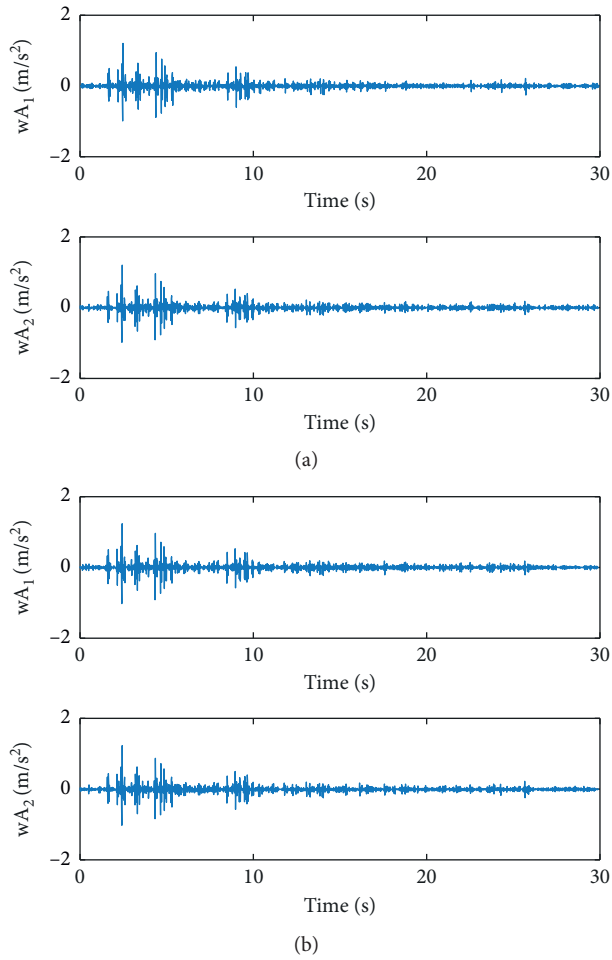

Figure 12: Wavelet detailed components of the simulated structure under E1-Centro earthquake wave. (a) Case 1. (b) Case 2.

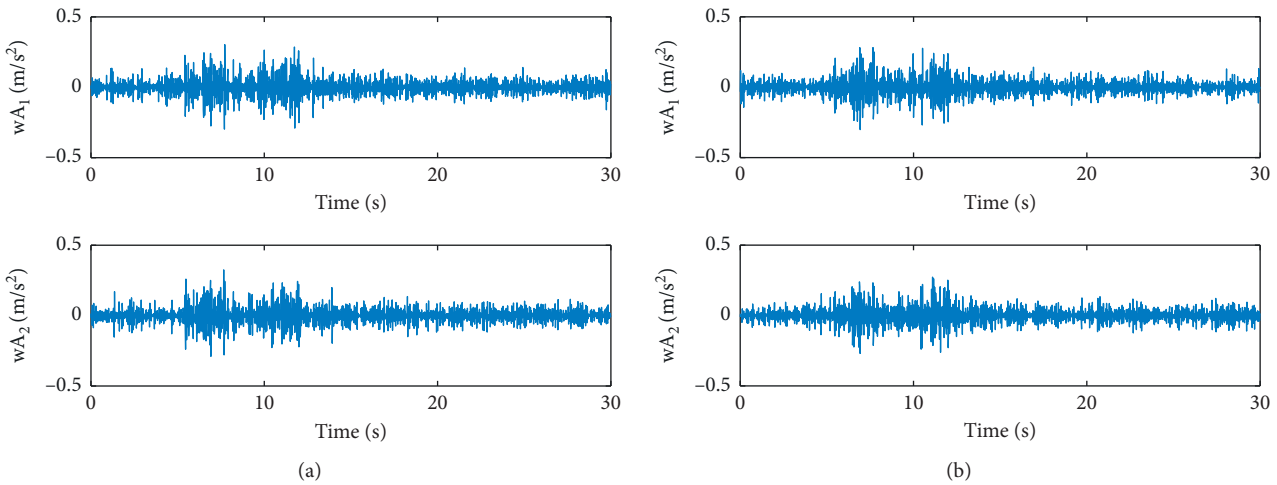

Figure 13: Wavelet detailed components of the simulated structure under Kobe earthquake wave. (a) Case 1. (b) Case 2.

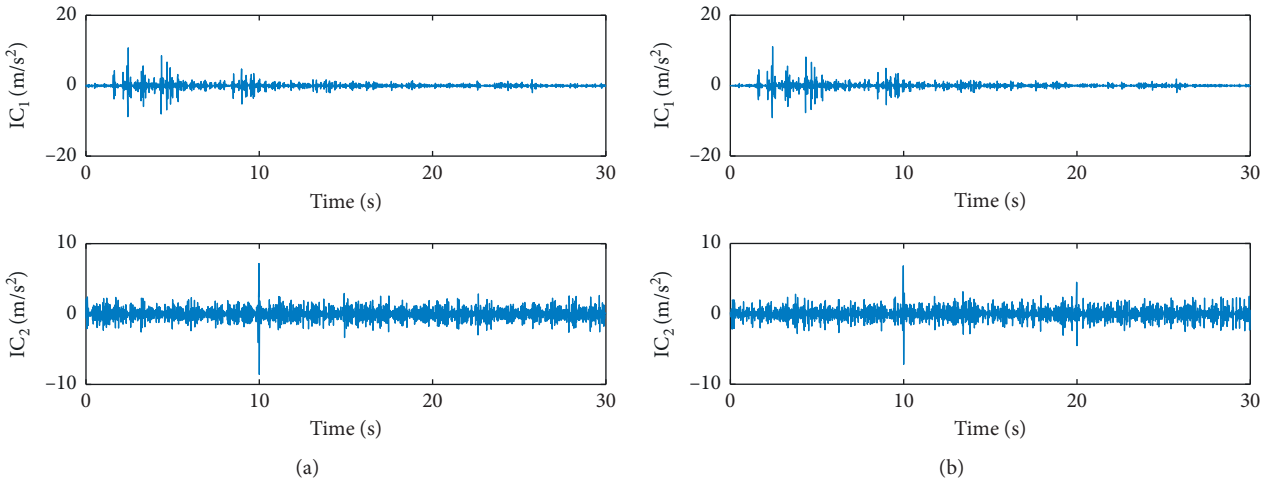

Figure 14: Independent component of the simulated structure under El-Centro earthquake wave. (a) Case 1. (b) Case 2.

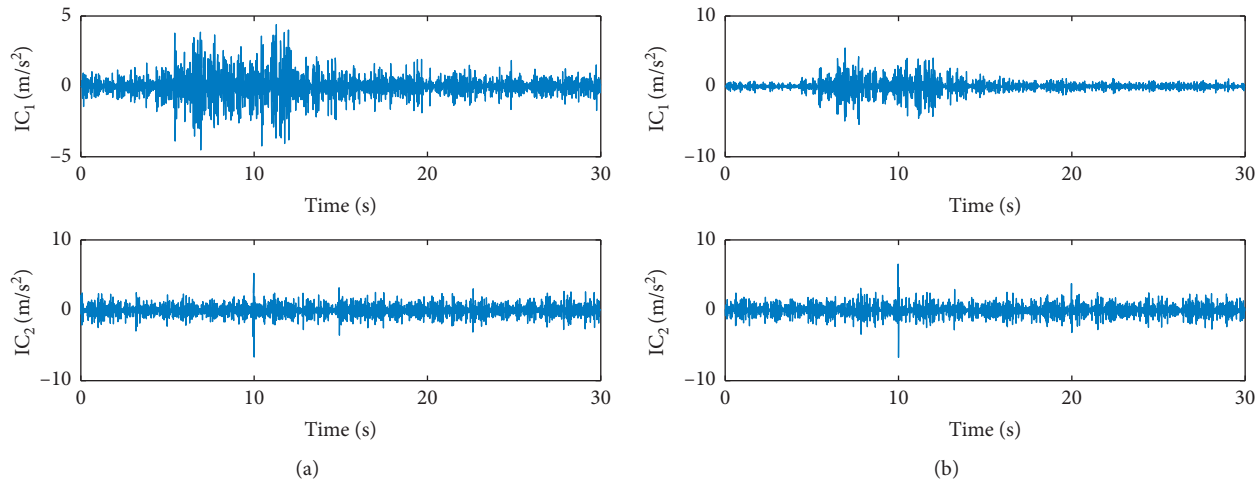

Figure 15: Independent component of the simulated structure under Kobe earthquake wave. (a) Case 1. (b) Case 2.

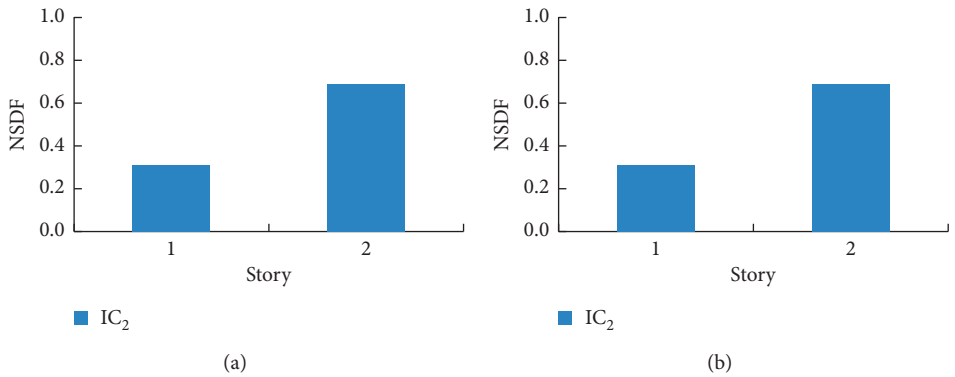

Figure 16: NSDV of the FIC under different earthquake waves. (a) EI-Centro earthquake. (b) Kobe earthquake.

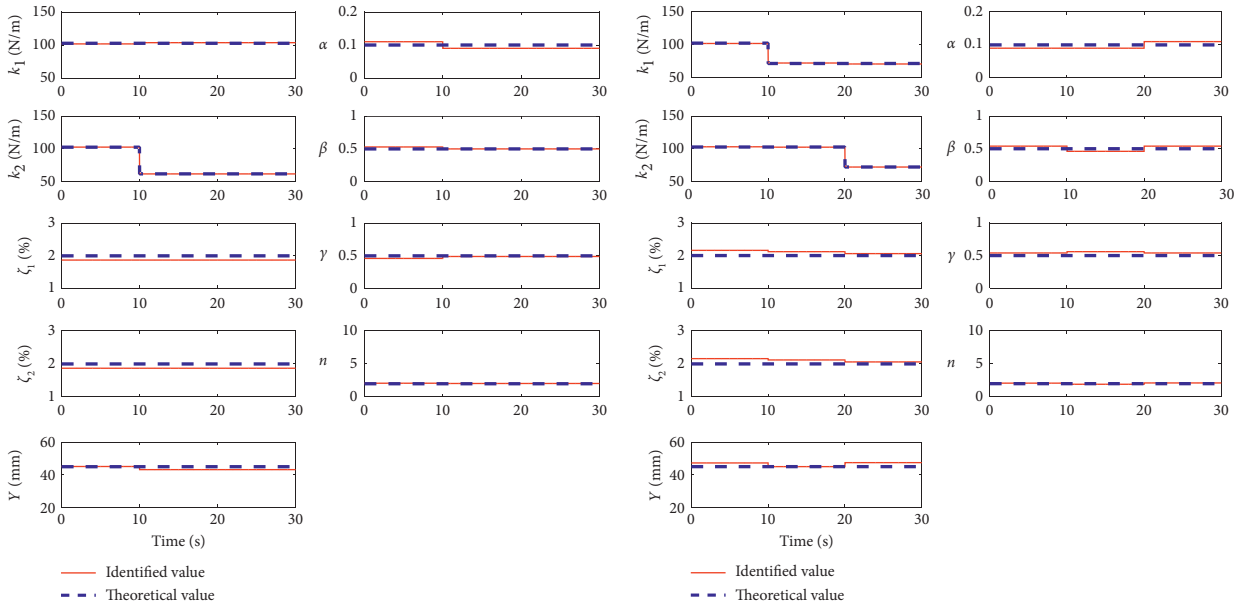

Figure 17: Structural parameters' identification results when structure is subject to EI-Centro earthquake. (a) Case 1. (b) Case 2.

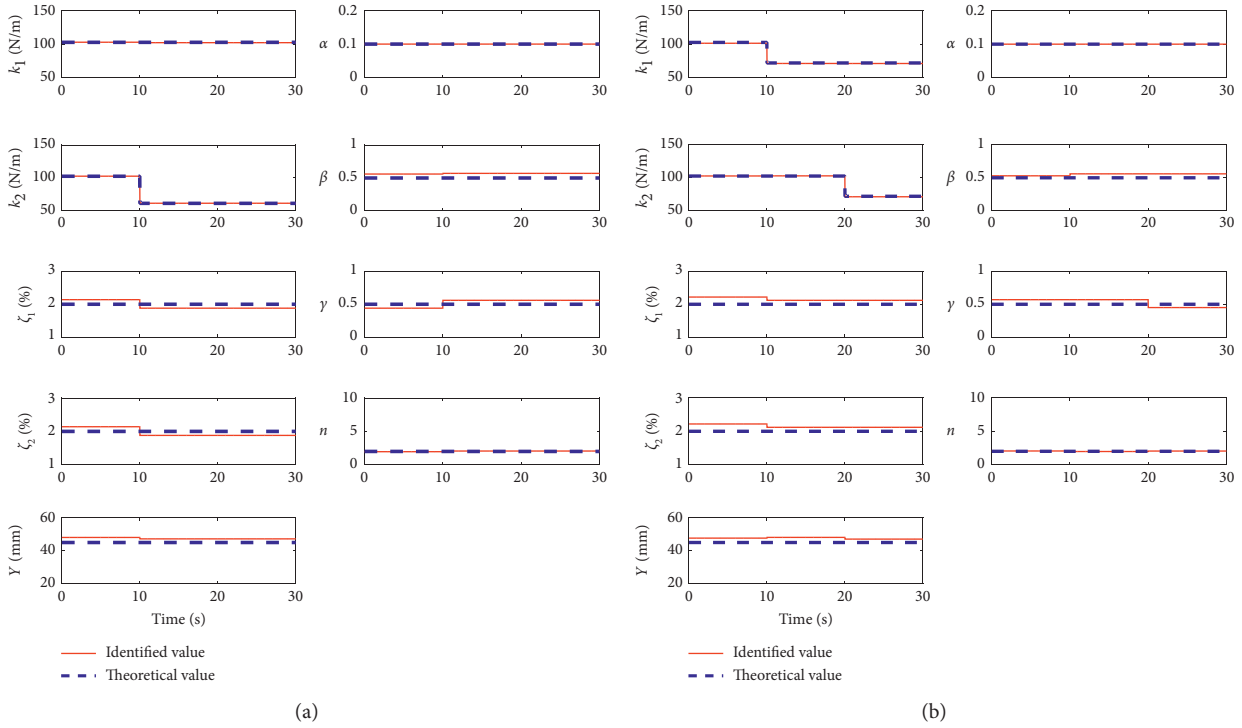

Figure 18: Identification results under Kobe earthquake wave. (a) Case 1. (b) Case 2.

Table 10: Relative errors between identification results and theoretical values under El-Centro earthquake wave.

Case	Time (s)	Relative error (%)								
		k_1	k_2	ζ_1	ζ_2	Y	α	β	γ	n
Case 1	0~10	0.93	0.12	6.50	8.50	0.29	10.00	6.00	8.00	4.00
	10~30	0.89	0.10	6.50	2.00	4.00	10.00	0.00	2.00	2.00
Case 2	0~10	0.49	0.35	8.00	8.00	5.07	10.00	8.00	8.00	4.00
	10~20	0.96	0.23	6.00	9.00	0.02	10.00	8.00	12.00	4.50
	20~30	1.08	0.07	3.00	8.00	5.49	10.00	8.00	8.00	5.50

Table 11: Relative errors between identification results and theoretical values under Kobe earthquake wave.

Case	Time (s)	Relative error (%)								
		k_1	k_2	ζ_1	ζ_2	Y	α	β	γ	n
Case 1	0~10	0.15	0.10	7.00	8.50	6.82	0.00	12.00	12.00	2.00
	10~30	0.51	0.29	6.00	7.50	4.91	0.00	14.00	12.00	3.00
Case 2	0~10	1.25	0.14	11.00	8.00	5.93	0.00	6.00	14.00	2.50
	10~20	1.10	0.29	6.00	9.00	6.91	0.00	12.00	14.00	1.50
	20~30	1.17	1.04	6.00	7.50	4.60	0.00	12.00	10.00	2.00

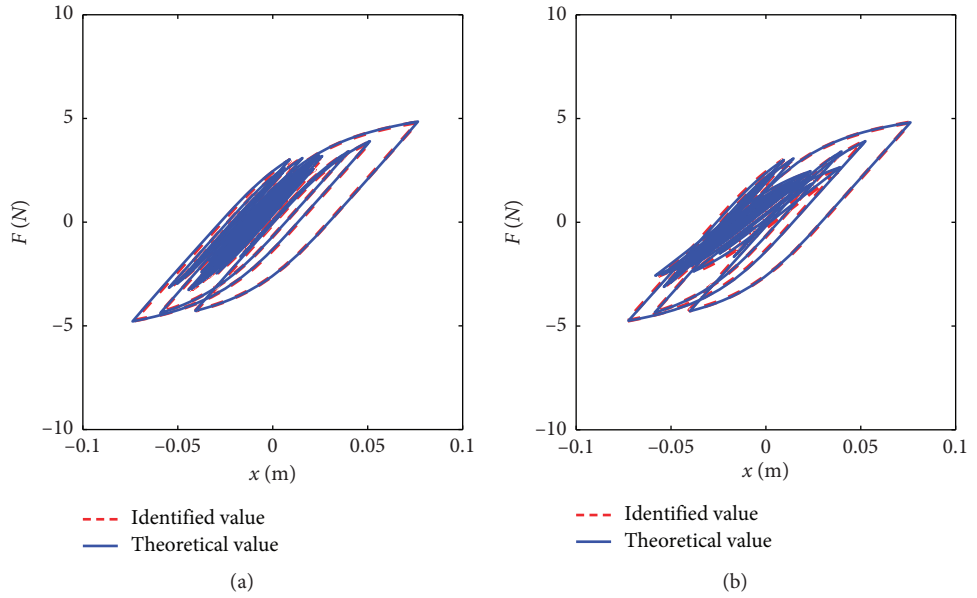

Figure 19: Comparison of hysteresis loops under EI-Centro earthquake wave. (a) Case 1. (b) Case 2.

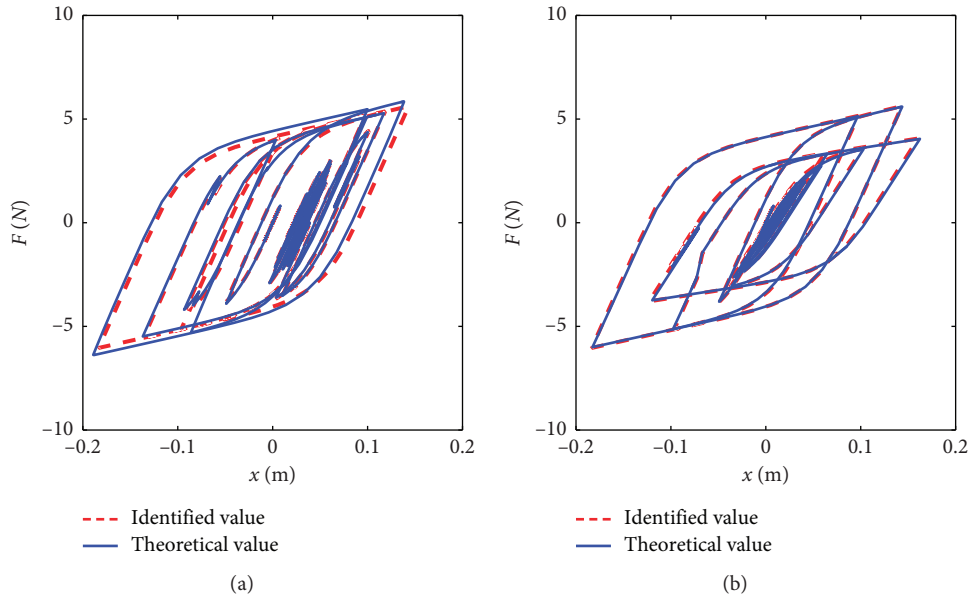

Figure 20: Comparison of hysteresis loops under Kobe earthquake wave. (a) Case 1. (b) Case 2.

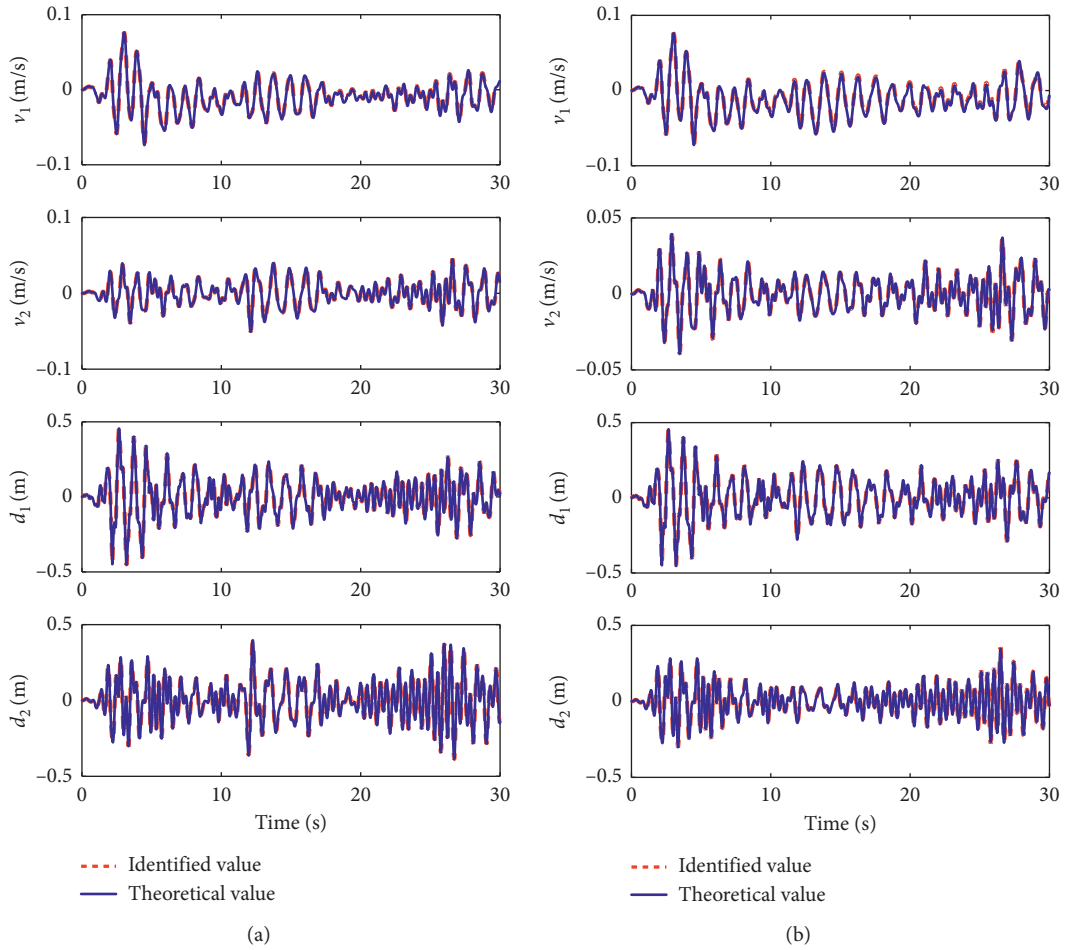

Figure 21: Comparison of velocities and displacements under El-Centro earthquake wave. (a) Case 1. (b) Case 2.

All in all, it can be seen that the identification results of the structural stiffnesses agree well with the theoretical values in both cases. This indicates that the precise damage localization and accurate assessment of damage extent can be realized in the second stage. Despite the rest of identified parameters with certain errors, these error values are good within modeling and construction errors. This implies that the proposed two-stage identification method is applicable to detecting sudden stiffness change in the acceleration responses for the nonlinear structures.

5.3.3. Discussion. For the sake of further evaluating the proposed method, identified and actual hysteresis loops for the structure under different ground motions are shown in Figures 19 and 20, respectively. In addition, identified and actual velocities and displacements for the structure subjected to different earthquakes waves are depicted in Figures 21 and 22, respectively. As shown in these figures, even for the worst damage pattern, case 2, with sudden changes in stiffness, the identified hysteresis loops, velocity, and displacements are in very good agreement with the actual values.

The identification results presented in this study are functionally equivalent to real-time results. Specifically, using software MATLAB R2015b, it took 8.96 s for each piecewise step of 10 s (500 Hz sampling rate) on a 3.20 GHz Intel® dual-core desktop machine to identify two stiffness values, damping, and the combined Bouc–Wen model parameters. In addition, the identification process at each time step only relies on the prior time step values. Hence, the proposed algorithm can be readily used as an online SHM method. In other words, the proposed strategy is a good choice for identifying sudden stiffness change in the acceleration response of a nonlinear hysteretic structure.

6. Conclusions and Remarks

This paper proposes a two-stage damage detection strategy by combining the DWT-FastICA technology and the IMPSCO algorithm for detecting sudden stiffness change in the accelerations of nonlinear hysteretic structures. Numerical simulation and experiment are used to validate the efficiency of the proposed methods. Some conclusions can be drawn as follows:

(1) The proposed strategy can not only locate the structural damage initially and quickly but also

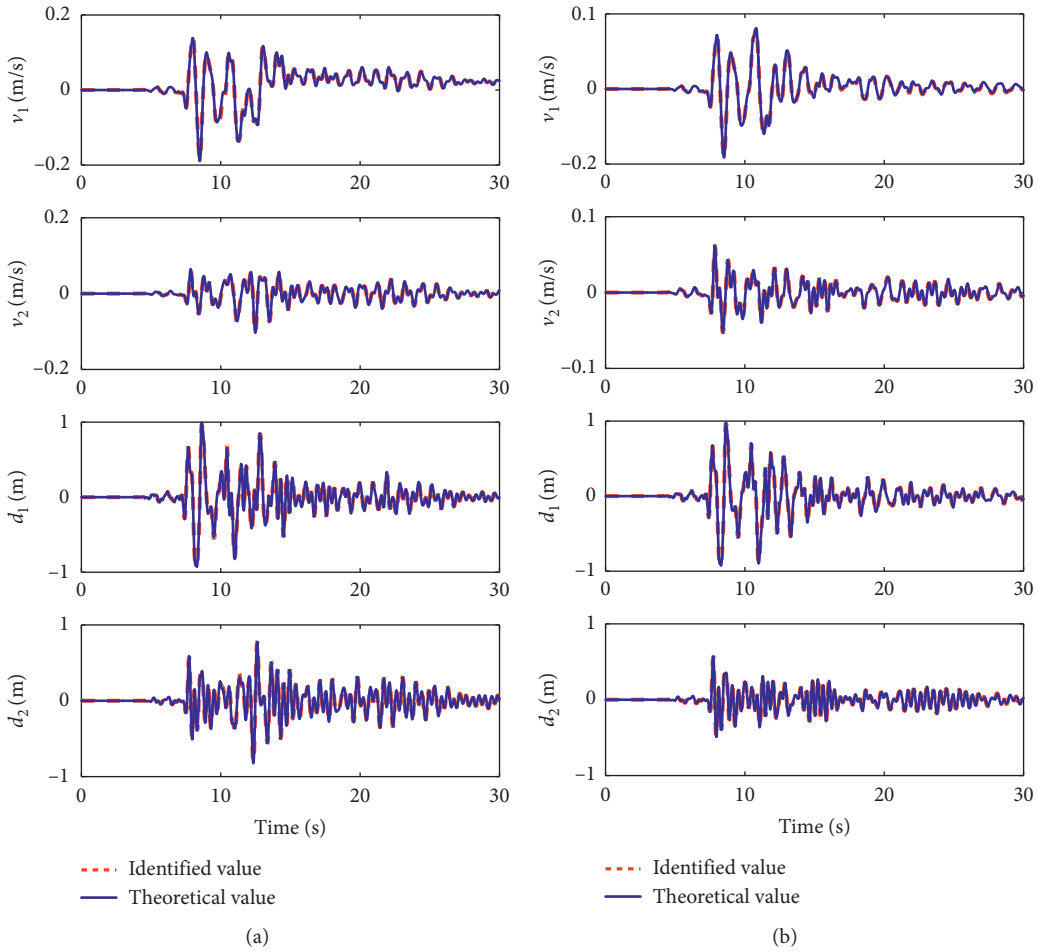

Figure 22: Comparison of velocities and displacements under Kobe earthquake wave. (a) Case 1. (b) Case 2.

quantify the damage severity accurately. It is noted that the proposed strategy is implemented only by using any kinds of structural time-series responses and does not require structural displacement measurements which are typically difficult to acquire or reasonably estimate.

(2) The IMPSCO algorithm is sui` to identify parameters in the modified Bouc–Wen model simulated by a MR damper, and the reconstruction force-displacement data can match well with relevant experimental data. The identification process at each time step based on IMPSCO is computationally efficient for sudden stiffness change in the acceleration response.

(3) The integration of DWT and Fast ICA can not only detect structural response novelty but also primary locate structural damage induced by stiffness change in time domain.

(4) The proposed strategy is applicable and effective for identifying key structural parameters including stiffness, damping, and the Bouc–Wen hysteretic model parameters with sudden stiffness change in the acceleration response. These parameters are directly related to well-recognized damage metrics.

(5) Proof-of-method simulations of a realistic nonlinear case-study structure, subjected to a suite of two different ground motions, show that the proposed method is well capable of identifying structural parameters to within 1.25% of the actual as-modeled values for stiffness.

In summary, it is effective and rapid to identify sudden stiffness change in the acceleration response of the two-story nonlinear Bouc–Wen model, and it still needs more experiments and structures to validate its efficiency in the future.

Data Availability

The data used to support the findings of this study are available from the corresponding author upon request.

Conflicts of Interest

The authors declare that they have no conflicts of interest.

Acknowledgments

The work was supported by the National Natural Science Foundation of China (grant nos. 51808119 and 51678156), the Science and Technology Major Project of the Science and Technology Department of Fujian Province (grant no.

2019HZ07011), and Open Funds of Fujian Provincial Key Laboratory of Advanced Technology and Informatization in Civil Engineering (grant no. KF-T18006).

References

[1] H. Aied, A. González, and D. Cantero, "Identification of sudden stiffness changes in the acceleration response of a bridge to moving loads using ensemble empirical mode decomposition," *Mechanical Systems and Signal Processing*, vol. 66-67, pp. 314–338, 2016.

[2] G. Boscato, L. Z. Fragonara, A. Cecchi et al., "Structural health monitoring through vibration-based approaches," *Shock and Vibration*, vol. 2019, Article ID 2380616, 5 pages, 2019.

[3] V. Ganesan, T. Das, N. Rahnavard, and J. L. Kauffman, "Vibration-based monitoring and diagnostics using compressive sensing," *Journal of Sound and Vibration*, vol. 394, pp. 612–630, 2017.

[4] Y. Lei, H. Zhou, and J. L. Li, "An on-line integration technique for structural damage detection and active optimal vibration control," *International Journal of Structural Stability and Dynamics*, vol. 14, no. 5, Article ID 1440003, 2014.

[5] J. Li and H. Hao, "Substructure damage identification based on wavelet-domain response reconstruction," *Structural Health Monitoring: An International Journal*, vol. 13, no. 4, pp. 389–405, 2014.

[6] Y. Yang and S. Nagarajaiah, "Blind identification of damage in time-varying systems using independent component analysis with wavelet transform," *Mechanical Systems and Signal Processing*, vol. 47, no. 1-2, pp. 3–20, 2014.

[7] S.-F. Jiang, D.-B. Fu, S.-L. Ma, S.-E. Fang, and Z.-Q. Wu, "Structural novelty detection based on adaptive consensus data fusion algorithm and wavelet analysis," *Advances in Structural Engineering*, vol. 16, no. 1, pp. 189–205, 2013.

[8] H. Mai, G. Song, and X. Liao, "Time-delayed dynamic neural network-based model for hysteresis behavior of shape-memory alloys," *Neural Computing and Applications*, vol. 27, no. 6, pp. 1519–1531, 2016.

[9] Y. Lei, Y. Wu, and T. Li, "Identification of non-linear structural parameters under limited input and output measurements," *International Journal of Non-linear Mechanics*, vol. 47, no. 10, pp. 1141–1146, 2012.

[10] L. Liu, W. Liu, and D. A. Cartes, "Particle swarm optimization-based parameter identification applied to permanent magnet synchronous motors," *Engineering Applications of Artificial Intelligence*, vol. 21, no. 7, pp. 1092–1100, 2008.

[11] A. Nickabadi, M. M. Ebadzadeh, and R. Safabakhsh, "A novel particle swarm optimization algorithm with adaptive inertia weight," *Applied Soft Computing*, vol. 11, no. 4, pp. 3658–3670, 2011.

[12] G. Quaranta, G. C. Marano, R. Greco, and G. Monti, "Parametric identification of seismic isolators using differential evolution and particle swarm optimization," *Applied Soft Computing*, vol. 22, no. 5, pp. 458–464, 2014.

[13] M. R. Senouci, D. Bouguettouche, F. Souilah, and A. Mellouk, "Static wireless sensor networks deployment using an improved binary PSO," *International Journal of Communication Systems*, vol. 29, no. 5, pp. 1026–1041, 2015.

[14] R. Machavaram and K. Shankar, "Joint damage identification using improved radial basis function (IRBF) networks in frequency and time domain," *Applied Soft Computing*, vol. 13, no. 7, pp. 3366–3379, 2013.

[15] A. E. Charalampakis and C. K. Dimou, "Identification of Bouc-wen hysteretic systems using particle swarm optimization," *Computers and Structures*, vol. 88, no. 21-22, pp. 1197–1205, 2010.

[16] J. Zhang and P. Xia, "An improved PSO algorithm for parameter identification of nonlinear dynamic hysteretic models," *Journal of Sound and Vibration*, vol. 389, pp. 153–167, 2017.

[17] A. Kunwar, R. Jha, M. Whelan, and K. Janoyan, "Damage detection in an experimental bridge model using Hilbert-Huang transform of transient vibrations," *Structural Control and Health Monitoring*, vol. 20, no. 1, pp. 1–15, 2013.

[18] J. I. Canelon, L. S. Shieh, and G. Song, "A new neural network-based approach for self-tuning control of nonlinear SISO discrete-time systems," *International Journal of Systems Science*, vol. 41, no. 12, pp. 1421–1435, 2010.

[19] J. L. Zapico, K. Worden, and F. J. Molina, "Vibration-based damage assessment in steel frames using neural networks," *Smart Materials and Structures*, vol. 10, no. 3, pp. 553–559, 2001.

[20] C. Zang, M. I. Friswell, and M. Imregun, "Structural damage detection using independent component analysis," *Structural Health Monitoring: An International Journal*, vol. 3, no. 1, pp. 69–83, 2004.

[21] S. L. Ma, S. F. Jiang, and L. Q. Weng, "Two-stage damage identification based on modal strain energy and revised particle swarm optimization," *International Journal of Structural Stability and Dynamics*, vol. 14, no. 5, Article ID 1440005, 2014.

[22] A. Hot, G. Kerschen, E. Foltête, and S. Cogan, "Detection and quantification of non-linear structural behavior using principal component analysis," *Mechanical Systems and Signal Processing*, vol. 26, no. 1, pp. 104–116, 2012.

[23] M. C. Constantinou and I. G. Tadjbakhsh, "Hysteretic dampers in base isolation: random approach," *Journal of Structural Engineering*, vol. 111, no. 4, pp. 705–721, 1985.

[24] E. K. Blum, "A modification of the Runge-Kutta fourth-order method," *Mathematics of Computation*, vol. 16, no. 78, p. 176, 1962.

[25] B. Niu, Y. Zhu, X. He, and H. Wu, "Mcpso: a multi-swarm cooperative particle swarm optimizer," *Applied Mathematics and Computation*, vol. 185, no. 2, pp. 1050–1062, 2007.

[26] M. Nayyerloo, *Real-time Structural Health Monitoring of Nonlinear Hysteretic Structures*, University of Canterbury Department of Mechanical Engineering, Christchurch, New Zealand, 2011.

[27] Z.-D. Xu, L.-F. Sha, X.-C. Zhang, and H.-H. Ye, "Design, performance test and analysis on magnetorheological damper for earthquake mitigation," *Structural Control and Health Monitoring*, vol. 20, no. 6, pp. 956–970, 2013.

[28] K. Worden and W. E. Becker, "On the identification of hysteretic systems. Part II: Bayesian sensitivity analysis and parameter confidence," *Mechanical Systems and Signal Processing*, vol. 29, no. S1, pp. 213–227, 2012.

[29] S. Mallat, *A Wavelet Tour of Signal Processing*, Academic Press, Cambridge, MA, USA, 1998.

[30] P. Comon, "Independent component analysis, a new concept?" *Signal Processing*, vol. 36, no. 3, pp. 287–314, 1994.

[31] A. Hyvärinen and E. Oja, "Independent component analysis: algorithms and applications," *Neural Networks*, vol. 13, no. 4-5, pp. 411–430, 2000.